KfK 3232
Oktober 1981

Energy Deposition of Ions in Materials, and Numerical Simulations of Compression, Ignition, and Burn of Ion Beam Driven Inertial Confinement Fusion Pellets

K. A. Long, N. A. Tahir
Institut für Neutronenphysik und Reaktortechnik

Kernforschungszentrum Karlsruhe

KERNFORSCHUNGSZENTRUM KARLSRUHE

Institut für Neutronenphysik und Reaktortechnik

KfK 3232

Energy Deposition of Ions in Materials, and Numerical Simulations of Compression, Ignition, and Burn of Ion Beam Driven Inertial Confinement Fusion Pellets

K. A. Long and N. A. Tahir

Kernforschungszentrum Karlsruhe GmbH, Karlsruhe

Kernforschungszentrum Karlsruhe GmbH
ISSN 0303-4003

Abstract

In this article various aspects of ion beam inertial confinement fusion are discussed. In particular a very thorough discussion of aspects of energy deposition of ions in hot plasmas and cold materials is given. Using energy deposition profiles given by these calculations, computer simulations of the compression, ignition and burn phases have been carried out for a single shell, pusher-tamper-DT fuel, multi-layered spherical pellet, suitable for use in a fusion reactor. The gain of this pellet was calculated to be 97 for an input energy of 7.38 MJ and an output energy of 715 MJ. This pellet has several other attractive features, including being environmentally attractive because of minimal radioactivity production and being insensitive to pusher-fuel instabilities.

Ionen-Energieverlust in Materialien sowie numerische Simulation der Kompression, der Zündung und des Abbrands eines ionenstrahlgetriebenen Fusions-Pellets basierend auf Trägheitseinschluß

Zusammenfassung

In diesem Bericht werden verschiedene Gesichtspunkte der Ionenstrahl-Trägheitseinschluß-Fusion diskutiert. Zunächst wird ausführlich der Energieverlust von Ionen in heißem Plasma sowie in kaltem Material erörtert. Dann wird unter Benutzung des so berechneten Energieverlustprofils eine numerische Simulation der Kompression, Zündung und des Abbrands für ein einschaliges, sphärisches Hohl-Pellet durchgeführt. Dieses einschalige Pellet besteht aus verschiedenen Schichten, und zwar aus einem Verdämmer, einem Treiber und aus Deuterium-Tritium-Brennstoff, so daß es für einen Fusionsreaktor besonders geeignet ist. Der Energiegewinn dieses Pellets errechnet sich als 97, und zwar für eine Eingangsenergie von 7,38 MJ und eine Ausgangsenergie von 715 MJ. Dieses Pellet hat noch einige andere attraktive Merkmale, so erweist es sich als umweltfreundlich wegen seiner geringen Radioaktivitätserzeugung und es neigt nicht zu Instabilitäten an der Treiber-Brennstoff-Grenzfläche.

Table of Contents

		page
1.	Introduction	1
2.	The physics and numerical methods of MEDUSA	2
3.	The importance of radiation and α-particle transport in ICF pellet simulations	7
4.	Energy deposition in the HIBALL pellet. The energy deposition code GORGON.	9
5.	Pellet gain calculations for the HIBALL reactor study using MEDUSA	21
6.	Discussion and conclusion	40
7.	References	42

1. Introduction

At the Institute for Neutron Physics and Reactor Technology, an advanced and extended version of the MEDUSA code is being used to design pellets for the ICF reactor study, HIBALL.[1] The design of pellets for ICF is a very complicated and involved problem and therefore use of a large computer code such as MEDUSA is essential. In order to be credible such a code must be carefully written and extensively tested on benchmark problems. The original version of the MEDUSA code was written by Christiansen, Roberts, and Ashby[2] at the Culham Laboratory, England. The code has been extended by Evans and Bell[3,4] of the Rutherford Laboratory (EOS, fast electron transport etc.), and by Tahir and Laing[5,6] of Glasgow University (radiation transport, ionization etc.). Further extensions have been made by Tahir and Long at KfK, Karlsruhe, in order to transform the code into a design code (multishell hollow pellets, radiation transport, ionization for heavy elements etc.) for ion beam fusion, and heavy ion beam fusion in particular. In section 2 the physics and numerical techniques of MEDUSA are presented. In this section the importance of realistic physics for accurate and meaningful simulations is stressed, in particular the fact that a realistic EOS is essential. In section 3 the effect of radiation transport on pellet simulations is discussed. The energy deposition of ions in hot plasmas is treated in section 4, and in particular the deposition profile in the HIBALL pellet is presented. We have carried out extensive simulation studies of various pellets during the last year. First of all we present calculations of a pellet first proposed by Bangerter[7] for light ions. Using the MEDUSA code we have "reproduced" these results done at Livermore around 1976, which establishes the credibility of MEDUSA as a pellet design code. Finally the HIBALL pellet (4 mgms of DT and all) has been simulated and first results are presented in section 5. Various conclusions are drawn from these calculations and these are given in section 6.

2. The physics and numerical methods in MEDUSA

The MEDUSA code is a well-known and well-tested code, because an intermediate version of the code has been published. The code has however been improved and extended in many ways since this version appeared. The physics and numerical methods in the code are as follows,

1. The code is a one-dimensional Lagrangian code which calculates for plane, cylindrical and spherical geometry.

2. It is a THREE temperature code, one temperature each for ions, electrons, and thermal radiation. The ions and electrons need separate temperatures in order to give a correct treatment of shock heating. In laser produced plasmas there is a very large difference between electron and ion temperatures in the underdense corona region. Further during the burn phase the ion temperature becomes considerably higher than the electron temperature, so this is very important for an accurate study of the physics of the burn phase. It is important also that the radiation field have a separate temperature for reasons explained in section 3.

3. The thermal conduction is due to electrons and radiation and both are flux limited. Flux limited conduction is vital in regions where there are very large temperature gradients, for instance at the outside of the shell and during the burn phase.

4. The code treats any type of multishell, multimaterial spherical pellet, and can calculate single and double shell targets.

5. Fast electron transport is included as well as a treatment of the ponderomotive force. These facilities are necessary in laser driven targets.

6. Absorption routines for both laser and ion beam fusion are incorporated. At the present time the ion beam deposition is calculated using analytic formulae, in which the range and the deposition profile can be changed.

7. The energy deposition of α-particles produced during the burn is treated locally and the neutrons produced during the burn are allowed to escape freely.

8. The equation of state of the ions is the classical ideal gas EOS. The EOS of the radiation is that of black body radiation. The equation of state of the electrons is in general more important than that of the ions because there are more of them. In the original version of MEDUSA the electron equation of state was either that of an ideal gas or of a degenerate or non-degenerate (as the case may be) Fermi-Dirac gas. These equations of state have been replaced (although they are still available as options within the code) because they cannot handle problems such as ionization and motion of electrons within the atomic potentials of the ions plus bound electrons. The ionization energy for instance represents an important sink of energy which is then not available for compression. Radiation is another such sink, and both these points have been made very strongly by D. Henderson[8] in discussing the dangers of using over-simplified physics. A Thomas-Fermi EOS has therefore been made available and as further sophistication a corrected Thomas-Fermi model which includes quantum and exchange forces is available. This EOS produces a very good fit to the Los Alamos EOS tables[9], and further allows for the total pressure to be zero at solid densities, so that materials do not expand unphysically when they are cold. Studies that we have made show that with the use of an ideal EOS, unrealistically high gains can be produced (even without much tuning), which then disappear when the corrected Thomas-Fermi EOS is used. Figs. 1 and 2 show a comparison of the EOS used in MEDUSA for Pb and DT with those of the Los Alamos tables.

9. Ionization states are calculated by use of the SAHA equation, and the average ionization $\langle Z \rangle$ and average squared ionization $\langle Z^2 \rangle$ used in various transport coefficients are also calculated by the SAHA routine. The TRIP time dependent ionization and atomic physics package is also incorporated in the code.

The hydrodynamic and energy equations are solved numerically in MEDUSA. The equation of motion is treated explicitly while the energy equations are solved by the Cranck-Nicolson implicit method and Gauss's elimination scheme. Since the energy equations are non-linear an iterative scheme is used to check the convergence of the numerical solution. Typically 5 to 10 iterations are required for convergence. Since the equation of motion is solved explicitly, the time step must be restricted by the C.F.L. (Courant, Friedrichs, and Levy) condition. For reasons of accuracy, the time step is also monitored by the time variation of T_e and T_i.

A typical MEDUSA run without radiation transport takes up to 15 minutes of CPU time on an IBM 3032 computer when calculating the 4 mgm DT HIBALL pellet. With radiation transport (one group treatment) a typical run takes up to 30 minutes.

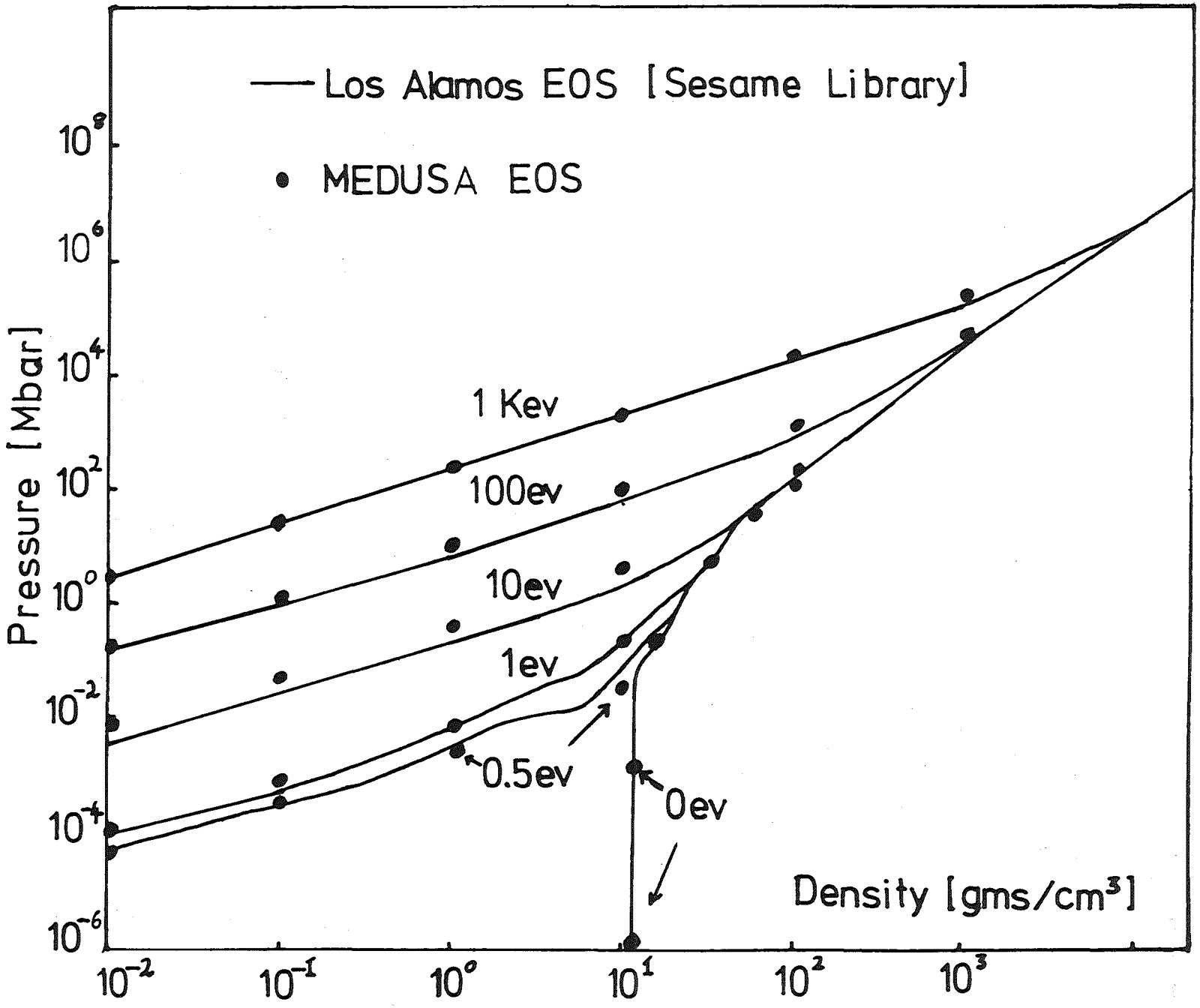

Fig. 1: Equation of state of Lead

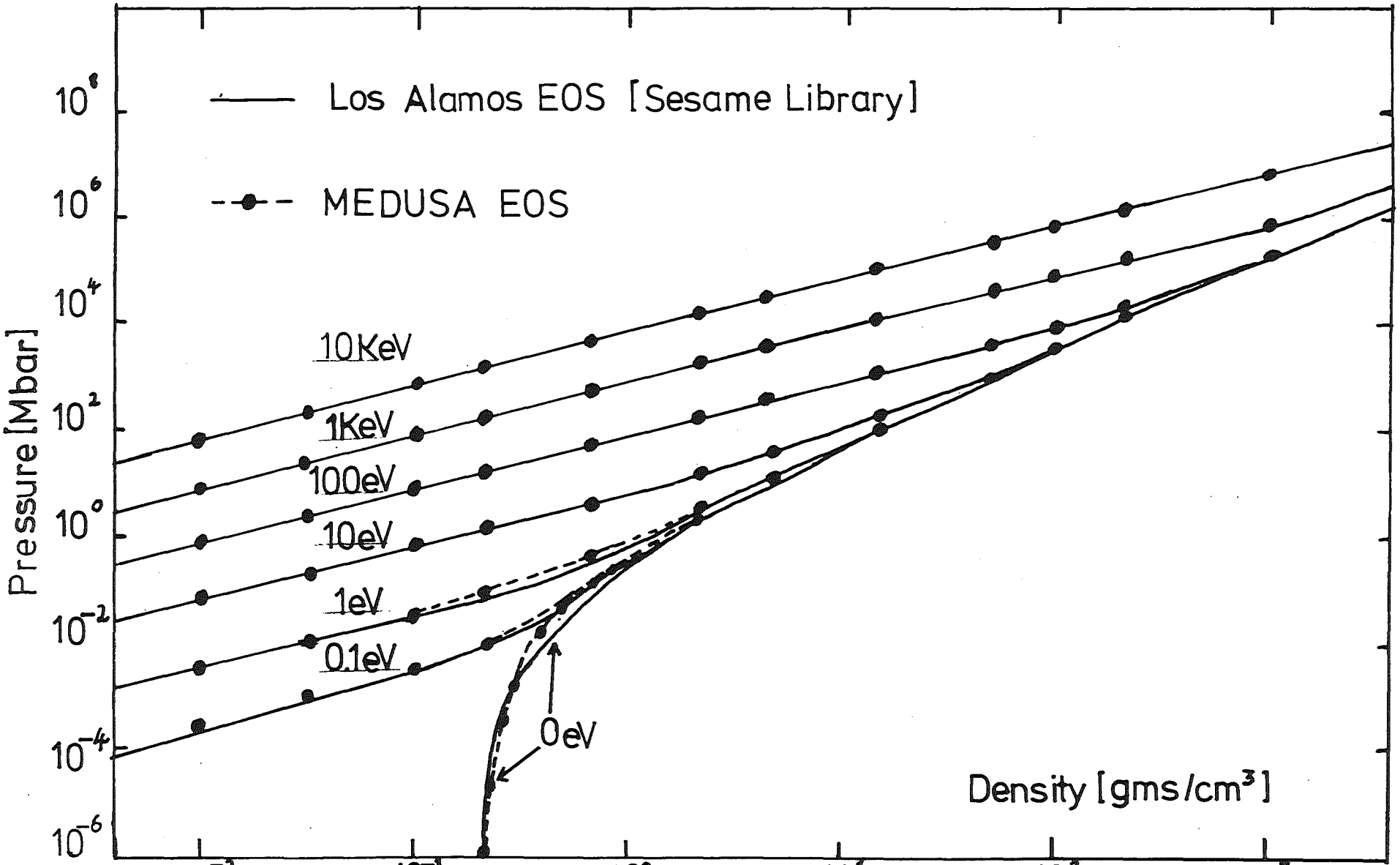

Fig. 2 Equation of state of DT

3. The importance of radiation and α-particle transport in ICF pellet simulations

Radiation effects can be of considerable importance in the ICF pellet simulations for the following reasons.

The thermal radiation produced by the thermal electrons in the absorption region can preheat the fuel and set the compression on a higher adiabat. This could degrade the final fuel density, which in turn, could reduce the target yield.

The thermal radiation may be helpful in smoothing out irradiation asymmetries.

The radiation losses from the target surface can be significantly large and may be reduced by an appropriate target design.

Radiation may be helpful to propagate thermonuclear burn from the ignition region into the surrounding dense and relatively cold fuel.

From the above considerations it is clear that the radiation can influence the compression and the burn propagation in an ICF target. It is, therefore, very important to include a radiation transport model in the hydrodynamic code, when designing a target for a reactor study. The updated version of the computer code MEDUSA used at KfK includes a steady state, single group radiation diffusion model which can simulate transport of total continuum radiation arising from free-free and free-bound transitions taking place in the plasma. This model has been developed by Tahir et al. [5,10] to simulate radiative preheat effects in laser-compression experiments performed at the Central Laser Facility, Rutherford Laboratory. Some typical results are published in [11,12].

It is to be noted that the applicability of the above model requires that the radiation field is in local equilibrium with the electrons. This assumption has limited validity in some stages of compression and burn of ICF pellets. A more accurate description

of radiation transport phenomena is given by a multi-group radiation model. In general, multi-group radiation transport models involve a large amount of the CPU time. When such a model is included in a hydrodynamic code, the CPU time requirements for the target simulations become prohibitively large. Tahir et al.[13] have proposed a multi-group treatment of radiation transport which will make use of the ICCG[14] numerical methods and will be very efficient compared to the standard multi-group models. The entire radiation field in this model is divided into a large number of groups (typically 20) which transport radiation energy in real space as well as in energy space. Diffusion in energy space takes place via electron-radiation interaction.

This model is being developed at KfK in collaboration with the Central Laser Facility, Rutherford Laboratory. We will incorporate this model into MEDUSA in order to take account of various radiation effects.

It has already been mentioned that in the MEDUSA code the α-particles are deposited at their place of origin. This means that the 3.6 MeV energy which they carry is deposited into the energy equation as a source term in the cell where they are produced. Clearly this is not correct and is a very bad approximation if the amount of DT is so small that α-particles can escape from the DT, for then the burn will not propagate. For large amounts of DT however practically all α-particles are absorbed and the burn front can propagate, and in this case the local α-deposition approximation is not too inaccurate. The energy of the α-particles is still retained in the DT but is distributed in a different manner from the true distribution allowing for the finite range of the α-particles. This can affect the detailed behaviour of burn propagation and the final fractional burn-up. It should be noted however that the burn can propagate even with local α-deposition via a blast wave due to the nuclear burn, electron conduction and thermal radiation. It is intended to extend the MEDUSA program by including a particle tracking[15] treatment of non-local α-particle deposition in the near future.

4. Energy deposition in the HIBALL pellet. The energy deposition code GORGON.

The distinguishing feature of ion beam fusion is of course that the energy is deposited by ions rather than from a laser. The original MEDUSA code was written as a laser fusion code and therefore modifications have to be made in order to transform it into an ion beam pellet design code. This is being done in two stages. The first stage consisted of using simple analytic formulae for $\frac{1}{\rho}dE/dx$ and these formulae are cold formulae. However one could expect that energy deposition would change considerably as the material heats up and forms a plasma consisting of free electrons and partially ionized atoms, since scattering from ions and electrons could be expected to be different than from neutral atoms. Hence one needs to develop a code based on a definite physical model that can calculate $\frac{1}{\rho}dE/dx$ as a function of density and temperature within the ranges of interest namely, 0 to 500 eV and ρ_s to $\rho_s/100$.* Then as a beam of ions is incident on a pellet, energy loss in each cell can be calculated as a function of the thermodynamic state of that cell, and this energy loss is then subtracted from the ion energy and the new energy is used to calculate dE/dx in the next cell. This procedure is continued until the ion energy is zero which then defines the range. The ranges of say protons in the 2 to 10 MeV range and heavy ions in the range 5 to 20 GeV are such that they are very well suited to implode pellets of the size to be encountered in I.C.F. This is not really surprising when one realises that the lower bound of the mass of DT in the pellet is fixed by the requirement that the hot burning pellet should reabsorb the α particles emitted in the DT reaction[16]. The upper bound is of course fixed by the size of the microexplosion that can be contained in a reactor chamber. A typical range for Bi^{++} in lead is $\sim 3 \cdot 10^{-2}$ gm/cm^2 or .3 mm, for a 10 GeV ion, whereas shell thicknesses for fusion pellets are of the order of 1/2 mm.

An energy deposition code, GORGON, based on Refs. 17 and 18 has been developed including modifications and extensions described below which are designed to deal with various physical effects.

* ρ_s is the solid density.

An ion travelling through a charged plasma, loses energy mainly to the electrons[19], by a series of small angle collisions. In each individual collision the amount of energy lost is very small, but because of the long range of the electrostatic forces, there are very many such collisions, so the total energy loss is quite large. The mass of the ion is much larger than the mass of the electron, so that the ion is deflected through small angles and one can consider the ion as travelling in a straight line. The projectile ion is further considered to be a point charge with specified energy, mass and charge (which may change with velocity, see below). The plasma is considered to be either degenerate or non-degenerate as the case may be.

The physical model used in the calculation is based on the distinction between the contribution of bound and free electrons in the target plasma. Free electrons are those having a wave function that extends to infinity (i.e. $\sim e^{i\underline{k}\cdot\underline{r}}$) and bound electrons are those whose wave function goes as e^{-kr} at large r, therefore not having infinite extent.

The contribution of the bound electrons to the stopping power is calculated according to Bethe's theory[20], taking into account the differences in characteristic excitation energies between a neutral atom and a plasma ion via the Thomas Fermi model. The contribution of the free electrons is calculated using the dielectric theory for non-degenerate electrons with a more simplified theory being used if the electrons are degenerate.

4.1 The physical model

(i) Calculation of the plasma parameters

In the model used in this calculation knowledge of the average degree of ionization in the plasma is required, because of the separate treatment of bound and free electrons. This is done using the Thomas-Fermi model of the atom at finite temperature. For this purpose the Thomas-Fermi model is solved using the

methods described by Latter[21], which yields values for the electron density distribution in the atomic sphere n(r) for a given density and temperature of the target material, as well as the potential V(r) and the chemical potential α. The number of bound electrons which yields the average degree of ionization is given in the Thomas Fermi model by,

$$N_b = \frac{32\pi^2}{h^3} \int_{-\infty}^{o} \frac{dE}{[\exp(E-\alpha)kT + 1]} \int_{o}^{r(E)} m[2m(E+eV(r))]^{1/2} r^2 dr \qquad (4-1)$$

where E is the total electron energy, m is the electron mass, T is the temperature, k is Boltzmann's constant, h is Planck's constant and r(E) is the radius which satisfies the condition,

$$eV(r(E)) = - E \qquad (4-2)$$

i.e. where the kinetic energy of the electron just equals its potential energy. From the number of bound electrons the number and density of the free electrons are determined and used in the calculation of the stopping power due to the plasma free electrons. The calculated structure of the ions is used to determine the bound electrons contribution to the stopping power.

(ii) Stopping power due to bound electrons

The contribution of bound electrons to the stopping power is calculated by Bethe's theory[22], including corrections due to the differences between a plasma ion and a neutral atom. The basic physical parameter is the average excitation energy I, defined by

$$\ln I = \frac{1}{N} \sum_i \ln(\hbar\omega_i) \qquad (4-3)$$

where N is the number of bound electrons participating in the slowing down process and $\hbar\omega_i$ are the characteristic excitation

energies. In these calculations the ω_i's are interpreted as the frequencies of revolution, following Bohr's model[23]. In order to calculate I within the framework of the Thomas Fermi model one notes that at each radius r a spectrum of revolution frequencies is determined by the Fermi energy distribution at this radius,

$$\omega(r) = [(2/m)\{E + eV(r)\}]^{1/2}/r \qquad (4\text{-}4)$$

Here E is the total electron energy. The number of electrons per unit frequency having a revolution frequency ω is,

$$n(\omega) = (32\pi^2\omega^2m^2/h^3)$$

$$x \int_o^{r_{max}(\omega)} r^5\left(\exp\left\{\left[\tfrac{1}{2}m\omega^2r^2 - eV(r) - \alpha\right]/kT\right\}+1\right)^{-1}dr \qquad (4\text{-}5)$$

Here $r_{max}(\omega)$ is the radius beyond which the energy which corresponds to ω yields a free electron, i.e.,

$$eV(r_{max}(\omega)) = - E \qquad (4\text{-}6)$$

The effective excitation energy is given, within the framework of this model, by

$$\ln I = \frac{1}{N}\int_o^{\infty} n(\omega)\ln(\hbar\omega)d\omega \qquad (4\text{-}7)$$

A shell correction is included in the calculation by eliminating from the integration in Eqn. (4-7) those electrons for which

$$2mv^2 < \hbar\omega \qquad (4\text{-}8)$$

where v is the projectile velocity.

The solution of the Thomas Fermi model, provides the required

values of V(r) (the potential), α (the chemical potential) and n(r) the electron density required in the above integrations.

(iii) Stopping power due to free electrons

The free electron contribution to the stopping power is calculated using the plasma dielectric theory[24,25,26]. The energy loss is given by,

$$\frac{dE}{ds} = - \frac{2e^2 Z_{eff}^2}{\pi\rho} \int_o^\infty kdk \int_o^1 \mu d\mu \; Im \left(\frac{1}{D(k,\omega=k\mu v)} \right) \qquad (4\text{-}9)$$

where ρ is the density, $s = \rho x$ where x is a distance into the material, v is the projectile velocity, k is the wave number, $\mu = \cos\theta = \underline{k}\cdot\underline{v}/|\underline{k}\cdot\underline{v}|$, D is the dielectric function of the plasma and ω is the frequency. In calculating the dielectric function a classical, non-degenerate plasma is assumed, and collisions in the plasma are taken into account. The collision time is given by,

$$\tau = 3m^{1/2}(kT)^{3/2}\left[4(2\pi)^{1/2}e^4 Z_{eff} n \ln\Lambda\right]^{-1} \qquad (4\text{-}10)$$

where n is the free electron density, Z_{eff} is the average ion charge, $\ln\Lambda$ is the Coulomb logarithm. The dielectric function is given by

$$D(k,\omega) = 1 + 2x^2\{1 + xZ(\xi)\}\omega_p^2/\omega^2 \; . \qquad (4\text{-}11)$$

where $\xi = x+iy$, $Z(\xi)$ is the plasma dispersion function, $x = \omega/kV_t$, $y = \nu/kV_t$, ν is the collision frequency, V_t is the free electron thermal velocity, $V_t = \left(\frac{2kT}{m}\right)^{1/2}$. An upper cutoff wave number is used in the integration in eqn. (4-9) following Bethe[19],

$$k_B^{-1} = e^{-\gamma}\hbar/mV_t$$

$$\gamma = 0.5772 \qquad (4\text{-}12)$$

Certain additions to the code have been made recently in order to improve the physics in the code and to allow the code to calculate stopping powers for heavy ions. The model now includes an option which allows the calculation of the stopping power of ions in degenerate electrons. This is an important factor for calculating the cold range in metals where up to 5 electrons/atom can be degenerate. Experimental results exist only at room temperature, so the calculations are calibrated on cold material, and it is therefore important to calculate correctly in this limit. The code as described above calculates the stopping power of protons very well, because the charge on the proton does not change as it passes through the plasma. In principle it could capture an electron to become a neutral hydrogen atom but since the binding energy is only 13 eV collisions with electrons would prevent this. However for heavy ions say Bi^{++}, entering a plasma, collisional ionization occurs, as also does recombination. This is a dynamic process and it takes time for the ion to reach a steady state effective charge when it is travelling at a constant velocity. However since the velocity is changing continuously it is not clear that the charge state ever reaches a steady state, and it is likely that the effective charge problem should be treated as a dynamic problem. For simplicity in the code at the moment a steady state effective charge formula is used, which is derived by comparing the 'cold' experimental results to the Bethe formula. The effective charge is the given by[27],

$$Z_{eff} = Z_B \left[1 - 1.034 \exp(-137.\beta/(Z_B))^{0.69}\right] \qquad (4\text{-}13)$$

where Z_B is the charge of the ions in the beam, v is the velocity of the ion, and $\beta = v/c$, where c is the velocity of light.

A general formula for dE/dx has the form, (from bound electrons),

$$\frac{dE}{dx} = Z_{eff}^2 \omega_p^2 \frac{e^2}{v^2} \cdot L \qquad (4\text{-}14)$$

where ω_p is the plasma frequency, v is the velocity of the ion, and e is the electron charge. In Bethe's formula L has the form,

$$L_{BETHE} = \ln \left\{ \frac{2mv^2}{\hbar\omega} \right\} - \ln(1 - \beta^2) - \beta^2 \qquad (4\text{-}15)$$

where $\hbar\omega = I$ is defined above, and m is the electron mass. On the other hand the classical expression derived by Bohr is given by,

$$L_{BOHR} = \ln \left(\frac{1.123mv^3}{Z_{eff}e^2\omega} \right) - \ln(1 - \beta^2) - \beta^2/2 \qquad (4\text{-}16)$$

A quantum mechanical expression derived by Bloch[29] who attempted to reconcile the two approaches is given by,

$$L_{BLOCH} = \ln \frac{2mv^2}{\hbar\omega} - \frac{1}{2} \ln(1 - \beta^2) - \beta^2/2$$

$$+ \psi(1) - Re\psi \ (1 + iZ_{eff}\alpha/\beta) \qquad (4\text{-}17)$$

where ψ is the diagamma function, and α is the fine structure constant.

The Bohr approach is one which uses classical mechanics, and is based on the use of an impact parameter b. For b greater than some impact parameter b_1 collisions are treated as electromagnetic excitations of harmonic oscillators in a constant electric field produced by the passing ion. For $b < b_1$, ions are assumed to scatter from the electrons as if the electrons were free. The Bethe approach uses quantum mechanics and therefore uses momentum transfer to characterize collisions. It considers the ion wave function to be a plane wave of given momentum and treats the ion-atom scattering within the Born approximation. The Bloch approach reconciles these two theories. Bloch demonstrates that the distant collision part of the Bohr theory is valid quantum mechanically within the dipole approximation. Bloch again assumed that for $b < b_1$ the electrons are free, but relaxed the assumption that the ion should be described by a plane wave. The confinement of the electron within a cylinder of radius b_1 introduces transverse momentum components which

interfere with each other under the influence of the scattering potential. This leads to a scattering cross section which can be very different to the Coulomb cross sections for plane waves.

For very weak scattering b_1 can be large, and plane waves can be used and the Bloch formula tends to the Bethe formula. In the limit of strong scattering wave packets can be constructed which scatter as classical objects and the Bloch formula gives the same results as obtained by Bohr. This happens especially when Z_{eff} is large. In the code the problem is solved by using the larger of two minimum impact parameters, one the quantum impact parameter $\frac{h}{2mv}$ and the other the Bohr impact parameter $\left(\frac{e^2 Z_{eff}}{mv^2} \right)$, where v is the relative speed between ions and electrons. This effectively changes the Bethe formula over to the Bohr formula.

Another change to the code that has been made, is to include the scattering of the ion off the ions in the plasma. The standard expression originally developed by Chandrasekhar[28] is used. The code can calculate for any type of ion (from hydrogen to uranium) and on any type single element target material, and can be extended to treat mixtures in a simple approximation. Since the code can calculate energy deposition for an ion passing through a degenerate plasma, it can also calculate the energy loss of α particles in degenerate and non-degenerate DT.

The results presented here are confined to those relevant to the HIBALL reactor, and other results illustrative of the working of the code will be presented elsewhere[29]. In Figure 3 is shown the energy deposition profile of 10 GeV Bismuth ions on lead at 200 eV and in Figure 4 the deposition profile of 10 GeV Bismuth ions in lithium at 200 eV is shown. The deposition profile in the HIBALL pellet for 10 GeV ions is shown in Figure 5 The range of the ions decreases as the temperature increases from room temperature. Also the deposition profile becomes more peaked at the end of the range as the temperature increases. The reason for this is as follows: At room temperature the energy

deposition profile is relatively flat and this comes about because the Bragg peak type profile which would be calculated using Z_B^2 is flattened out by the decrease in Z_{eff}^2 as a function of velocity. As the range is shortened the cut off occurs at larger values of Z_{eff}^2, so that the flattening effect is much reduced and the Bragg peak starts to reappear. It should be noted here that the peak in the distribution curve always occurs when $V_B \sim V_{el}^{Th}$ (the electron thermal velocity), and as the temperature increases so does V_{el}^{Th}, so V_B becomes greater at this point and so does $Z_{eff}(V)$.

In conclusion the assumptions that are inherent in these calculations are briefly considered. The ion is assumed to travel in a straight line and lose energy by small angle scattering to the electrons by excitation and ionization. Hence large angle scattering events are ignored, as these are important only at lower energies. The ions are assumed to slow down independently of each other, that is collective effects (of the beam interaction) are assumed to be absent. This is justified by an argument proposed by Melhorn[30]. For typical beam parameters the interparticle spacing is >100Å, while the relevant shielding distance in both solid and plasma is of the order of 1Å. Hence in some sense the particles should not see each other. However this is not the whole story, since one should also consider the time domain. Ions going through a plasma emit plasmons which vibrate with a period $\sim 10^{-17}$ secs. Ions travel typically with a velocity $\sim 3 \cdot 10^9$ cm/sec, so the time taken to travel 100Å is $\sim 10^{-16}$ secs. Therefore as long as the plasmons are not damped out in $\sim$ 10 oscillations the next ion will see the perturbation produced by the ion in front. Under certain circumstances this could lead to bunching and a coherent motion of the ions, leading to the unstable growth of large amplitude plasma waves. This could then lead at least to enhanced energy deposition. This effect is currently being investigated to see if such an instability can occur within the parameter space relevant to ICF fusion.

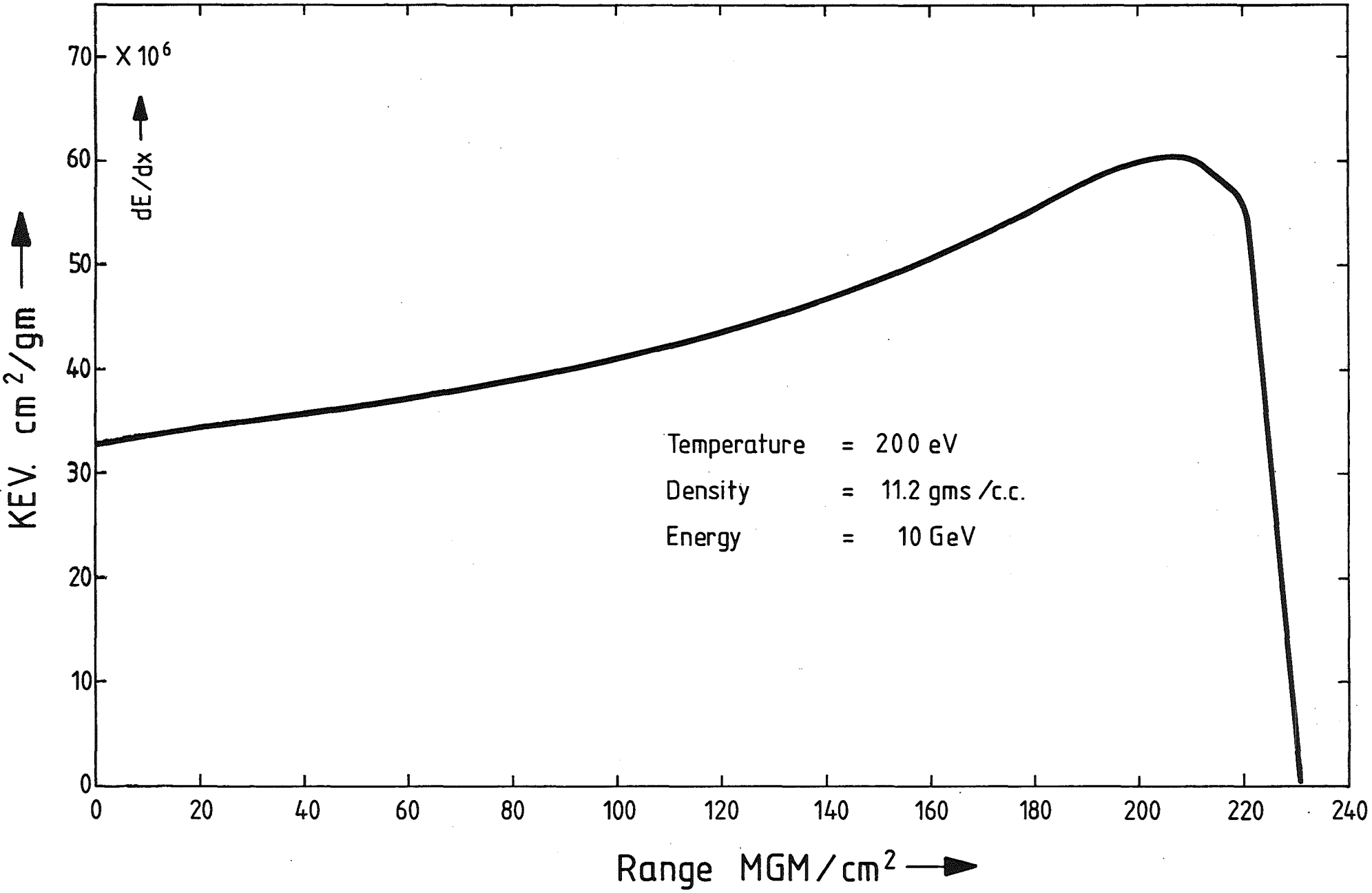

Fig. 3: Stopping power of bismuth ions on lead

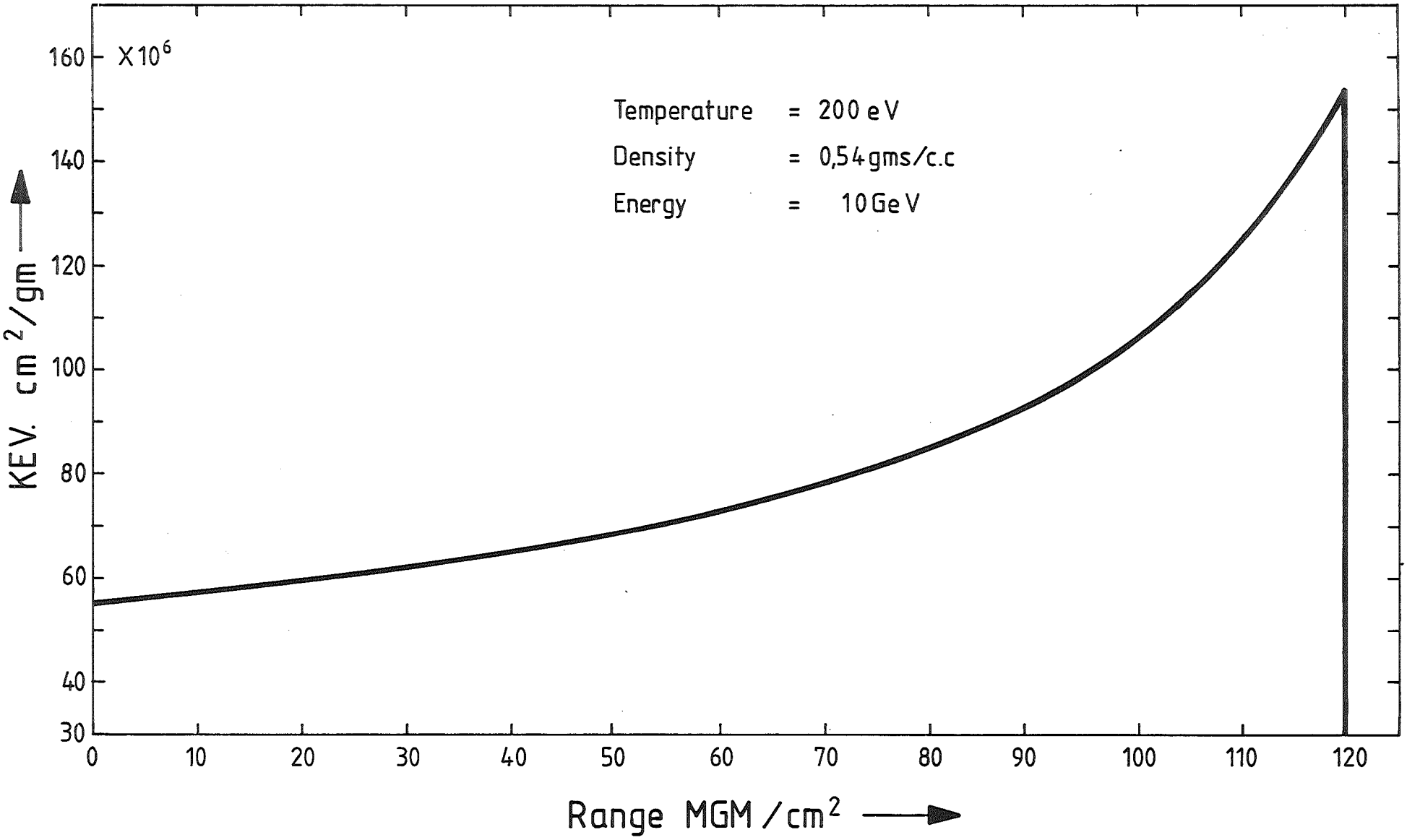

Fig. 4: Stopping power of bismuth ions on lithium

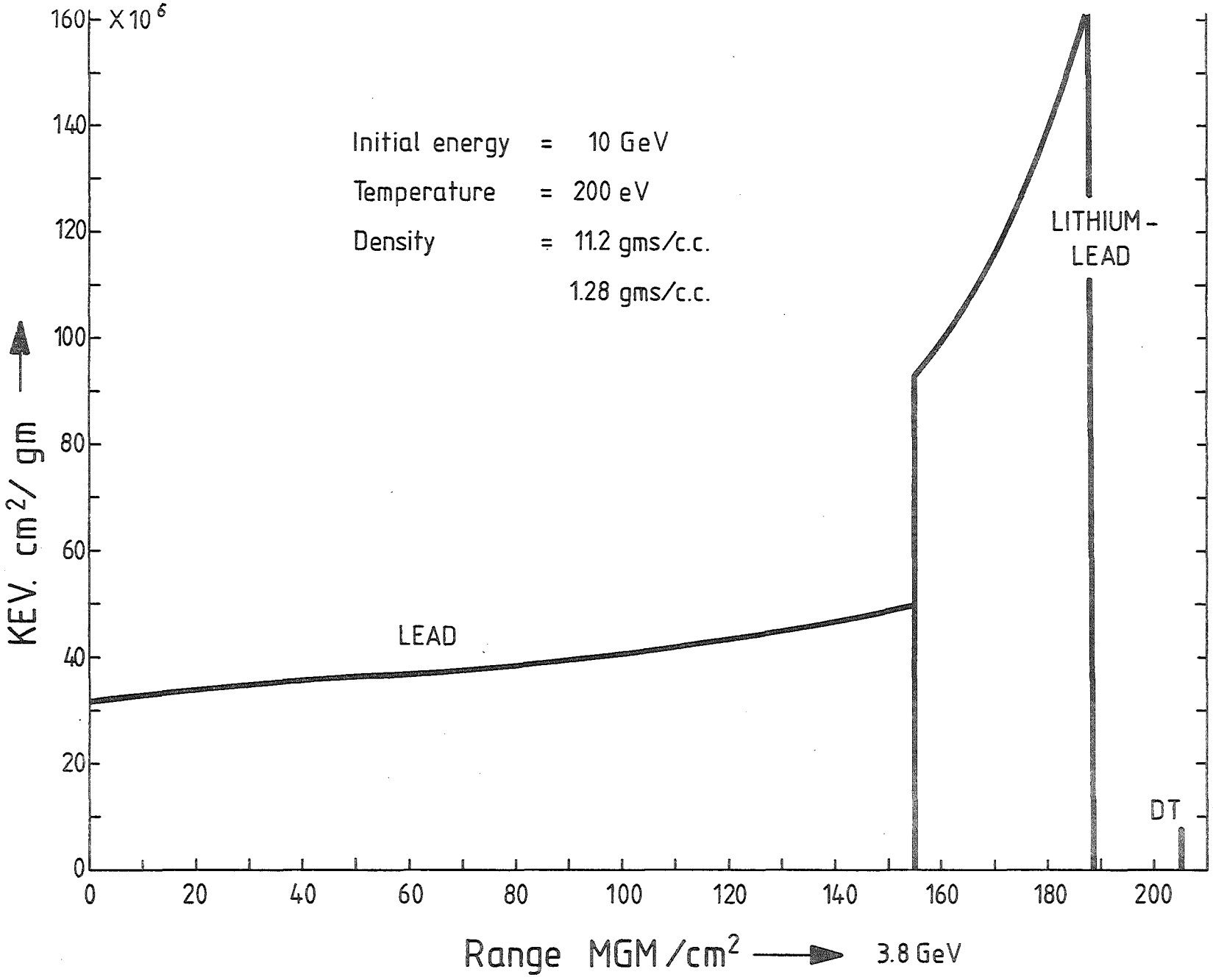

Fig. 5: Bismuth ions on lead and lithium - lead

5. Pellet gain calculations for the HIBALL reactor study using MEDUSA

The art of pellet design involves many different facets some of which are of a theoretical nature and some of which are of a practical nature. The initial idea involved in ICF[31,16] employed a solid DT microsphere which was to be isentropically compressed and ignited. This was then found to require large amounts of energy and power. In order to ameliorate this situation the use of DT shells was proposed, because since the shells would be given kinetic energy over a relatively long time which would at void closure be converted to internal energy of compression, the power requirements could be reduced[32,33]. The HIBALL pellet employs a cyrogenic DT shell but surrounded by layers of PbLi and Pb the purpose of which is explained below. In a reactor design it is essential to keep the recirculating fraction of energy as low as possible in order to minimize costs. Further the driver efficiency is likely to be for accelerators of the order of 25 %, so that the pellet gain must be high to compensate for these factors, i.e. $G > 40$. Considerations similar to those of Bodner[34] show that this rules out volume ignition of DT. One way to improve the situation was found to be to create only a central hot spot of small mass and isentropically compress the remaining DT, in such a way that the burn would spread from the central "spark" to the remaining fuel. This increases the gain because the energy needed to compress DT when $kT << \varepsilon_F$ (the Fermi energy) is much less than that required to heat nondegenerate DT to the same temperature. The question then is how to create such a spark, in other words what pulse shape does one need? As discussed by Kidder[35,36,37] one way of doing this is to launch a weak shock down the density gradient of the shell, and at the same time compress the shell in a homogeneous and isentropic manner. With real shells which have constant density this is not strictly possible but it can be done to a certain extent. The shock produces a hot spark region in the centre of the shell. This shock is produced by a prepulse of low power, and it breaks through the inner boundary after about 10 ns. The passage of the shock causes free-surface oscillations of the inner surface. The conversion of this energy into heat after void closure, followed by additional compression by the decelerating

matter surrounding the heated central region, leads to the formation of the central spark.
On the other hand the shock is weak enough not to shock heat the outer position of DT. When the radius of the shell has a certain value the main pulse is applied. This generates a very large pressure wave which compresses the DT, and also sends a second shock wave into the centre of DT helping to form the spark reigon. As the void closes the large pressure wave comes in to compress the central region of DT and a return shock propagates out of the spark region. This sequence as pointed out by Kidder[37] produces a density profile which is lower in the spark region by a factor up to 10 than the outer fuel region, a temperature which is higher by a factor up to 10 in the spark region and a region of roughly constant pressure over the spark region and the rest of the fuel behind the shock front. This is the point of ignition where the central hot spot has just ignited, and is about to propagate outwards. This it does if the energy created in the burn is greater than that lost by electron and radiation conduction. Normally the non-local α-particle deposition also helps to propagate the burn phase, but this effect cannot be seen in MEDUSA calculations since it considers local α-particle energy deposition.

It has already been mentioned that an ICF target should have a high gain, but there are several other requirements that it should fulfill. The target should be hydrodynamically stable and it should have a reasonable tolerance of irradiation asymmetries. It should also need as low an energy and power as possible to ignite it. Further certain other requirements should be met which do not directly involve target physics considerations. For instance the target should be easy to fabricate and should be made out of relatively cheap materials. It would be desirable that the target produces a minimal amount of radioactivity, that it should be compatible with other materials of the reactor coolant system and finally it should be large enough so that the beam can be focussed onto it.

Many of the above requirements impose contradictory constraints. For example, power requirements can be reduced by using shells

with large aspect ratio, but such shells tend to be fluid-dynamically unstable.
Bangerter and Meeker[7] proposed a target which fulfills most of the above requirements and is shown in Fig. 8. This is a single shell multi-layered target with a low density, low Z pusher sandwiched between a high density, high Z tamper and the fuel. The heavy tamper serves as a confinement shell to increase the efficiency of implosion. The pusher is seeded with a high Z material to reduce radiative preheat of the fuel. The use of a low density pusher has a number of advantages over a high density pusher. For instance, the pusher can be made relatively thick to reduce hydrodynamic instabilities and yet contain little mass. Also the hydrodynamic instabilities causing pusher-fuel mixing during the final stages of compression may be eliminated because of the very small density difference between the fuel and the pusher. In addition, this target has a simple structure and is made from inexpensive materials. The simulations of Bangerter and Meeker[7] indicate that in the case of a high Z pusher target comparable to the one shown in Fig. 8 (but without TaCOH), the ρR in the pusher is 10 gms/cm^2. In the present calculations, on the other hand, the bulk of the high Z material remains uncompressed and the total ρR of both the pusher and the tamper is less than 1 gm/cm^2. The latter target would therefore produce less than 10 % as much high Z radioactive debris as a target with high Z pushers.

As a first step towards designing the HIBALL[1] pellet we simulated the 1 mgm DT Bangerter-pellet[38] with the updated version of MEDUSA. To make these calculations computationally simpler we replaced the TaCOH pusher by PbLi, the two have the same mass density and approximately the same electron number density. Our results show good agreement with the Bangerter-Meeker results. It is, however, to be noted that a pellet with 4 mgs of DT is required for the HIBALL reactor study. For this purpose we scaled the above pellet to a bigger pellet which contains 4.3 mgs of DT in such a way that the two pellets have the same aspect ratios. From now on we shall refer to this bigger pellet

as the "HIBALL PELLET". We have simulated the compression, ignition and the burn propagation in this HIBALL pellet. The results for the 1 mgm DT pellet and the HIBALL pellet are discussed below.

Results

a) 1 mgm DT pellet (Comparison between Bangerter-Meeker and KfK results)

The pellet shown in Fig. 8 has been calculated by Bangerter and Meeker using the pulse shape and deposition profile shown in Fig 6 and Fig. A2 of ref. 38 respectively. This pulse shape is designed to compress this target in such a manner that the inner 10 % of the fuel is shock heated and compressed by the prepulse while the main pulse compresses the surrounding DT isentropically on a relatively low adiabat. The central hot region then ignites and sends an outgoing shock through the surrounding dense and cold fuel, thereby spreading the burn throughout the fuel. The electron and the radiation thermal conduction as well as the non-local α-particle deposition also help in spreading the burn through the target[39,40,41].

We simulated a very similar target, but with PbLi pusher instead of TaCOH, as shown in Fig. 9. The two materials have the same mass density and approximately same number of electrons/unit volume. We have used approximately the same deposition profile as in Fig. 5. The pulse shape used in our calculations is shown in Fig. 7 and is relatively simple compared to the one used by Bangerter and Meeker. We give a comparison between our results and the Bangerter-Meeker results in Table 1.

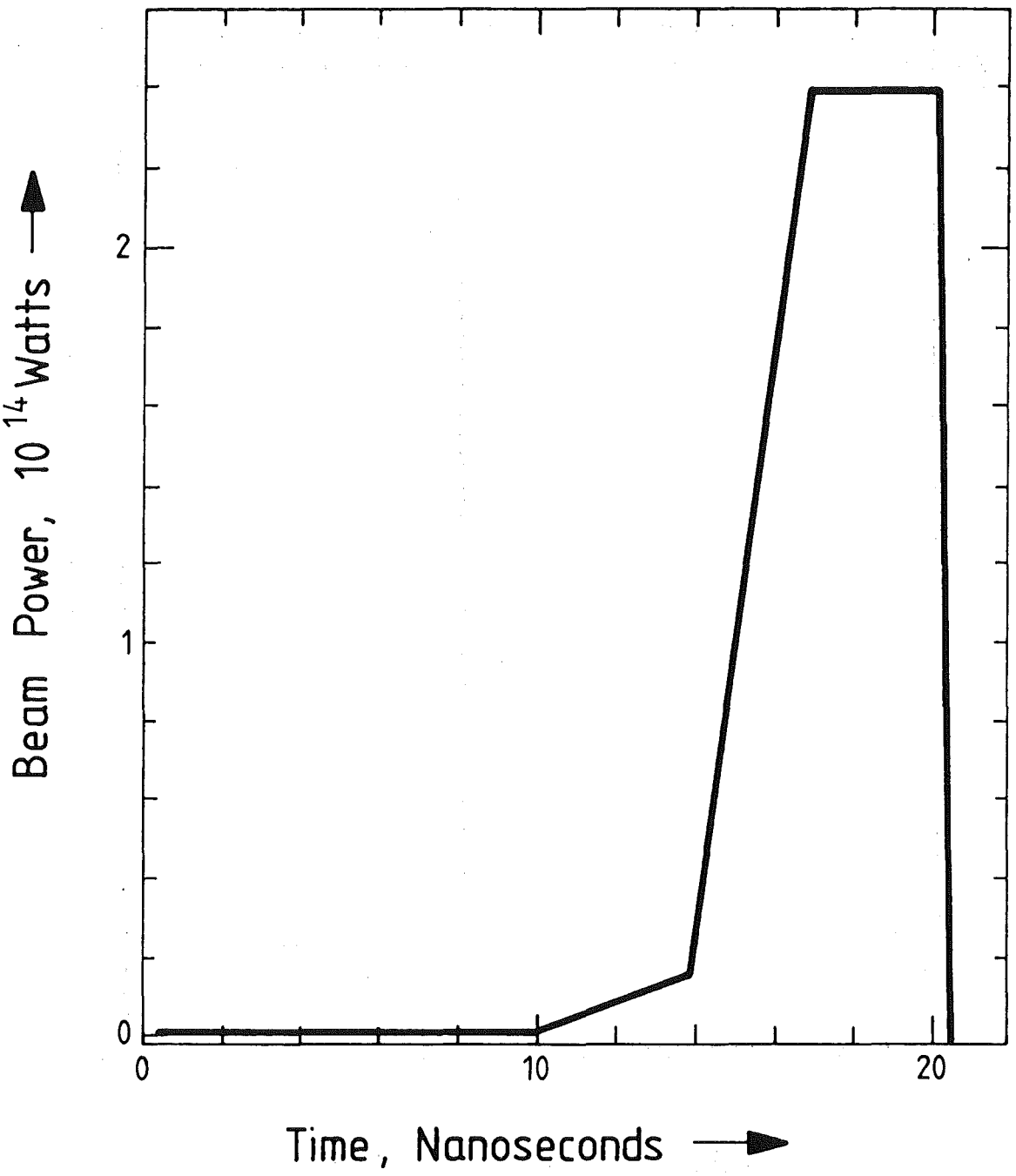

Fig. 6: Pulse used by Bangerter and Meeker Ref. 36 for 1 mg pellet

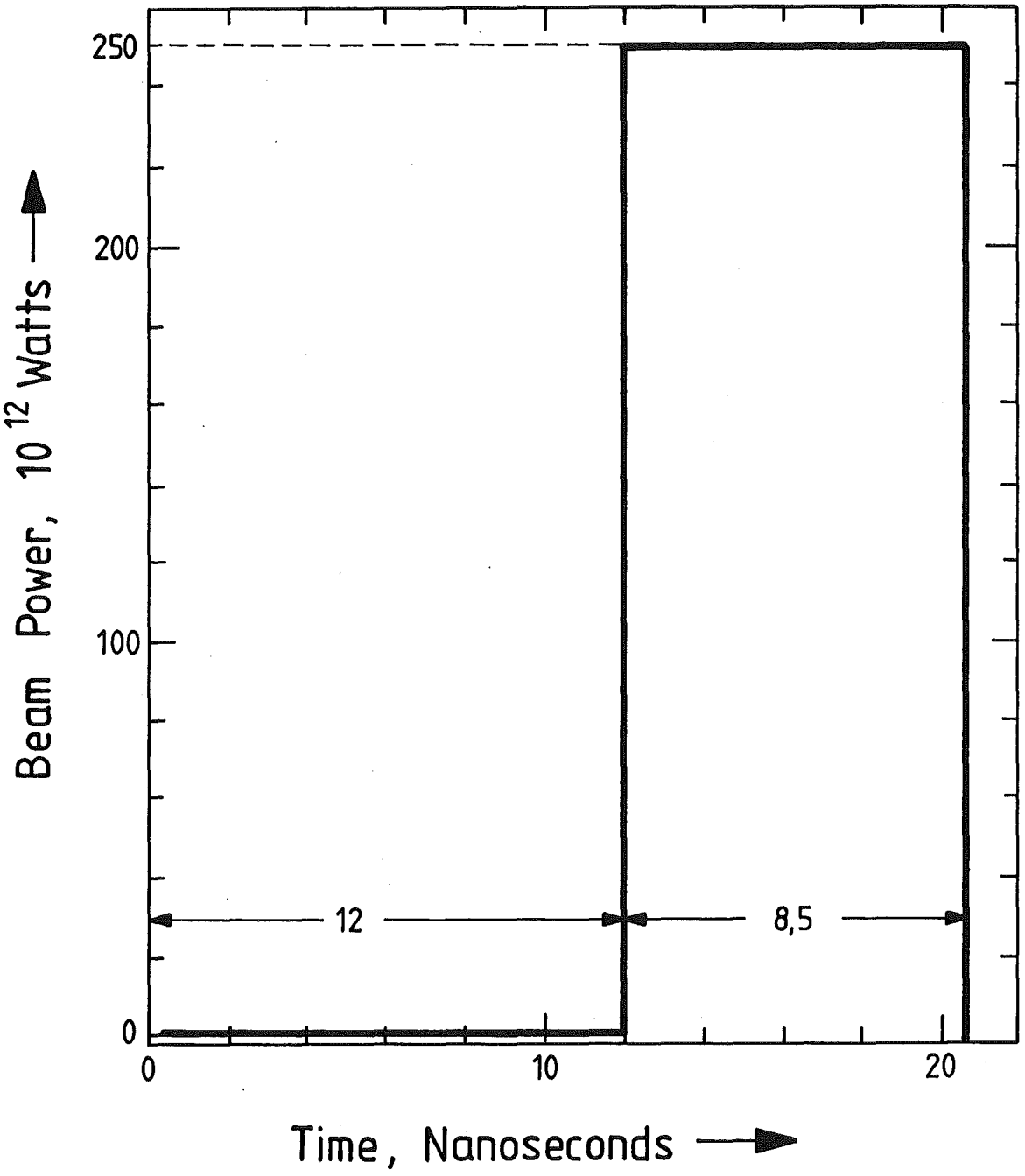

Fig. 7: Beam power as a function of time

Table 1: Comparison between Livermore and KfK results

	Bangerter-Meeker	KfK
Pulse Energy (MJ)	1.28	2.0
Peak Power (TW)	240	250
Output Energy (MJ)	113	164
Gain	88	84

From the above table it is seen that Meeker and Bangerter have obtained a gain of 88 by using less input energy and practically the same peak power. To get a gain comparable to their value we had to use somewhat higher input energy. The reason for this is that they have used a shaped pulse in their calculations which is designed to minimize shock heating of the fuel. Their target is compressed on a lower adiabat and the input energy requirement is reduced. We, on the other hand, have used a relatively simpler pulse, shown in Fig. 7. This pulse shape gives rise to more shock heating of the target and so the compression is placed on a higher adiabat. Consequently, we require more energy to achieve a high pellet gain. We have used 2 MJ input energy in our calculations which compresses the target to give a higher value of ρR as compared to the Bangerter-Meeker calculations. As a consequence we get more fractional burnup of DT and a larger output energy.

We also note that during the final stages of compression the fuel density becomes comparable to the pusher density which is very good for the stability of the pusher-fuel interface. This effect has also been mentioned by Bangerter and Meeker[7,38].

b) The HIBALL pellet with 4.3 mgs DT

Using the updated version of MEDUSA described in section 2, we have simulated compression and ignition of the HIBALL pellet shown in Fig. 9. We have also studied the problem of burn propagation from the central spark region into the surrounding dense and cold fuel.

To design an ICF target and tune it for maximum output energy for a possible minimum input energy and power is a very complicated and time consuming problem. The reason for this is that the designer has to work in a multi-dimensional parameter space. The most basic parameter in this space is the type of the target itself which can either be a single shell multi-layered or a composite shell multi-layered target. For the HIBALL pellet we chose a single shell multi-layered target with the same structural design and aspect ratio as the 1 mg target shown in Fig. 8. The next set of variables which one has to select, are the input energy, the pulse shape and the pulse parameters. Bangerter[38] has mentioned an approximate energy mass scaling relationship according to which one should use 20 to 25 MJ/gm for good target compression. Applying this scaling law our target would require 7.5 MJ input energy.

We used a pulse shape similar to the one shown in Fig. 7. The choice of correct pulse parameters is another difficult problem. Since each computer run takes about 15 - 20 minutes of the IBM 3032 computer at KfK, it was not possible to vary these parameters blindly (to tune the pellet). We guessed the prepulse and the main pulse lengths to scale according to $m^{1/3}$ times the corresponding values for 1 mg pellet. The pulse parameters used in our calculations and the target yield are given in Tables 2 and 3 respectively.

We have used simple analytic formulae to simulate heavy ion deposition in the pellet. The target conditions at the time of ignition are shown in Fig. 10.

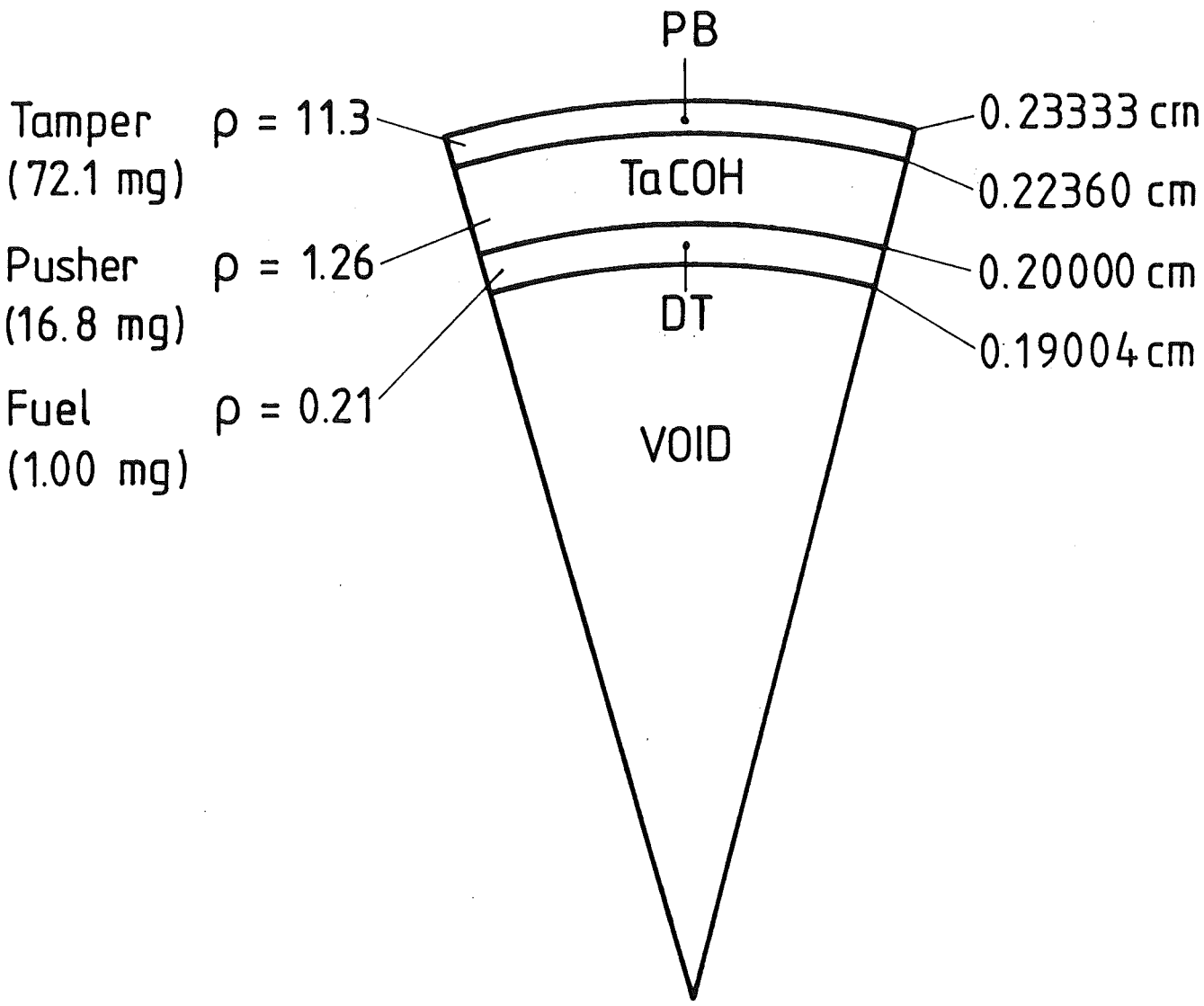

Fig. 8: Initial configuration of 1 mg pellet

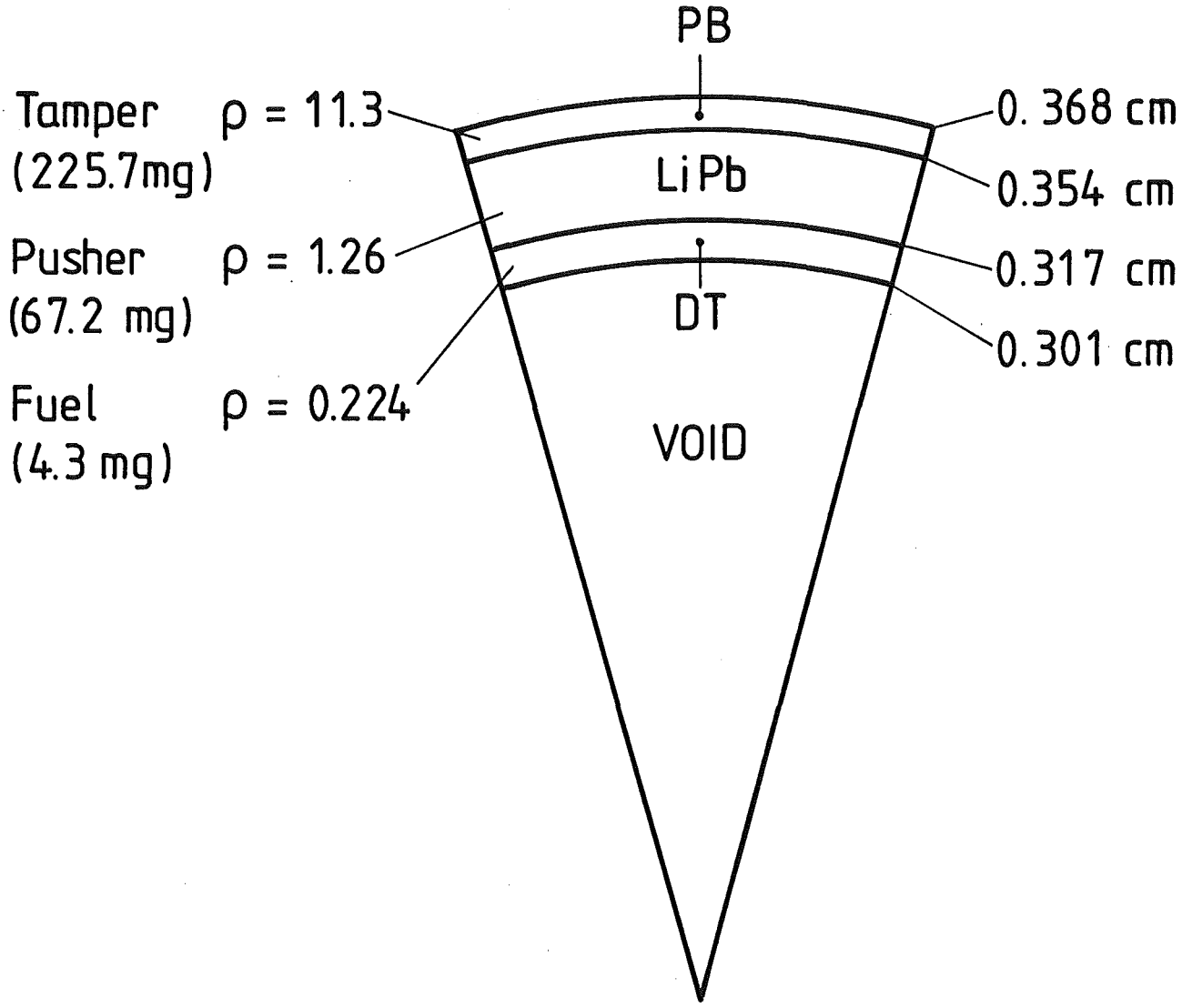

Fig. 9: Initial configuration of 4.3 mg HIBALL pellet

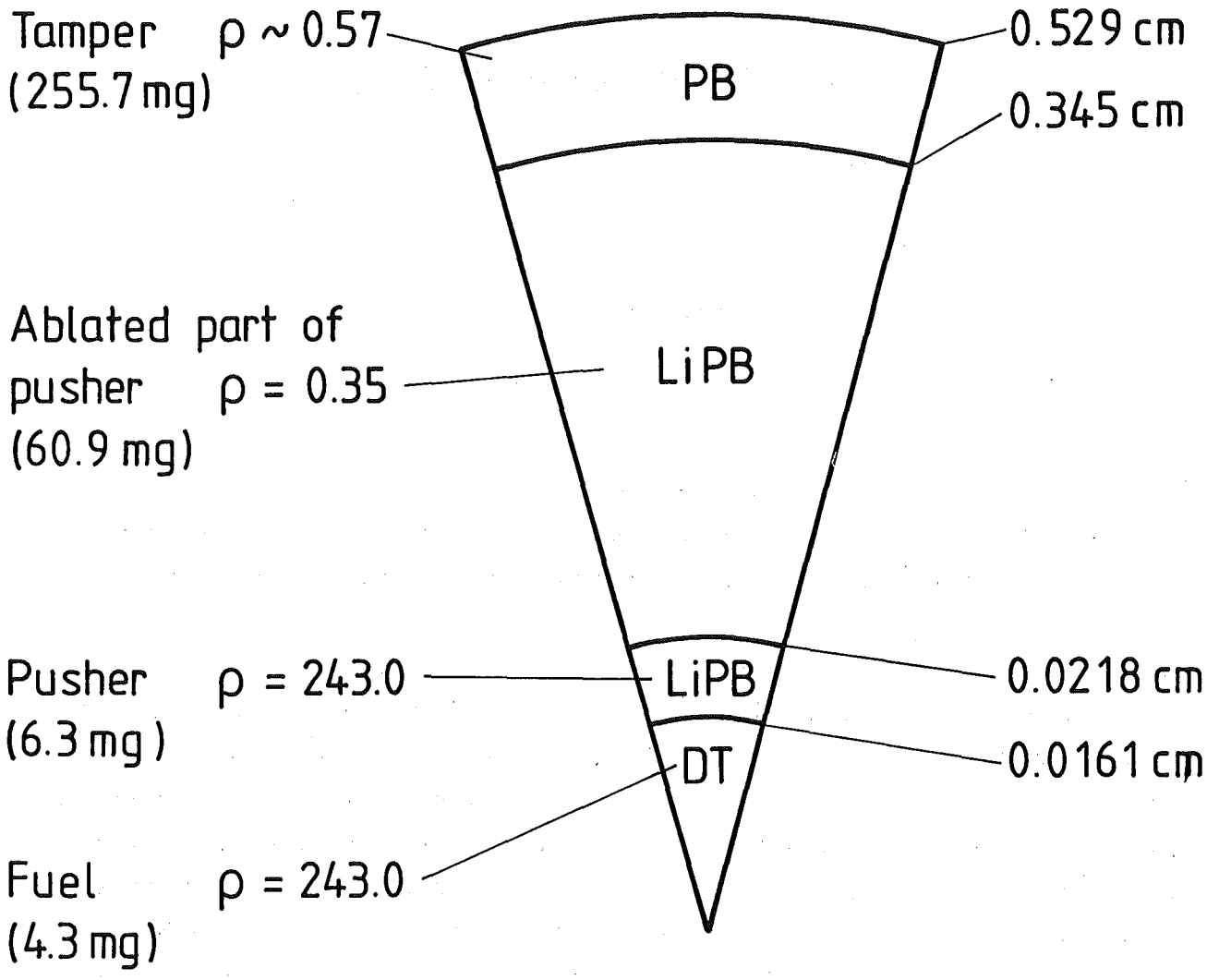

Fig. 10: Ignition state of HIBALL pellet

Table 2: Pulse Parameters

Prepulse Power	10 TW
Main Pulse Power	600 TW
Prepulse Length	18 ns
Main Pulse Length	12 ns

Table 3: Input Energy and Target Yield

Pulse Energy (MJ)	7.38
Gain	97
Output Energy (MJ)	715

The performance of this target could be improved substantially by further fine tuning. The target yield can be optimized with less input energy and lower peak power by using a shaped pulse.

It should also be noted that one-dimensional codes cannot treat the hydrodynamic instabilities and the effects arising from non-uniform target illuminations. These effects can be studied by two-dimensional codes. Inclusion of the above two effects may degrade the compression substantially which in turn would reduce the target output. According to Meeker* two-dimensional simulations of a typical target show a reduction in gain compared to the gain obtained by one-dimensional calculations for the same target.

In Fig. 11 the co-ordinates for the tamper-pusher and pusher-fuel interfaces are plotted respectively as a function of time. It is seen that the pusher-fuel interface moves inwards as the target gets compressed and ignition starts at about t = 31.0 ns. This is the time when compression achieves its maximum value and this time corresponds to the switch off time of the pulse.

* D. Meeker, Private Communication

The tamper-pusher interface on the other hand maintains a steady position during the burn phase and then moves outwards as the target expands. This is because the tamper is very heavy and it does not move in but holds the pusher and the fuel together for a time long enough so that nuclear fusion takes place.

The ignition and burn conditions are given in Figs. 12 to 14. We plot $\log\rho$, $\log P$ and $\log T_i$ as a function of the pellet radius at three different times. The solid and broken vertical lines represent the pusher-fuel and the pusher-tamper interfaces respectively. Fig. 12 is plotted at t = 31 ns when the compression has achieved its maximum value. It is seen that the inner 10 % of the fuel is heated to ignition temperature but is at a relatively lower density such that the total pressure in the fuel is constant. Fig. 13 is plotted after 130 ps and it shows a pressure peak in the ignited fuel region. This is because the charged particles produced in the nuclear reactions deposit their energy and heat up the fuel to temperatures $\sim 10^8$ K. This pressure peak sends a shock wave into the surrounding fuel and the burn spreads radially throughout the fuel. It is seen from Fig. 14 that after 150 ps the whole of the fuel is heated to a temperature $\sim 10^9$ K. We note that in these calculations we do not include radiation transport effects because of the unavailability of opacities for lead. Since the pusher in this pellet is seeded with a high Z element, the radiative preheat effects will be reduced. Also the surface temperature of the target is $\sim$ 100 eV and so the radiation losses will be small. In these calculations we have neglected radiation losses. However, inclusion of radiation transport will help the burn propagation. We expect to include radiation effects in our future calculations of the HIBALL pellet.

In Fig. 15 we plot the Atwood number at the pusher fuel interface as a function of time. It is seen that towards the end of the implosion the Atwood number decreases rapidly and even becomes negative. This indicates that while the pusher is being

decelerated by the high pressure in the fuel, the fuel density becomes comparable to the pusher density. This indicates that our target should be stable to hydrodynamic instabilities which cause pusher-fuel mixing during the final stages of implosion.

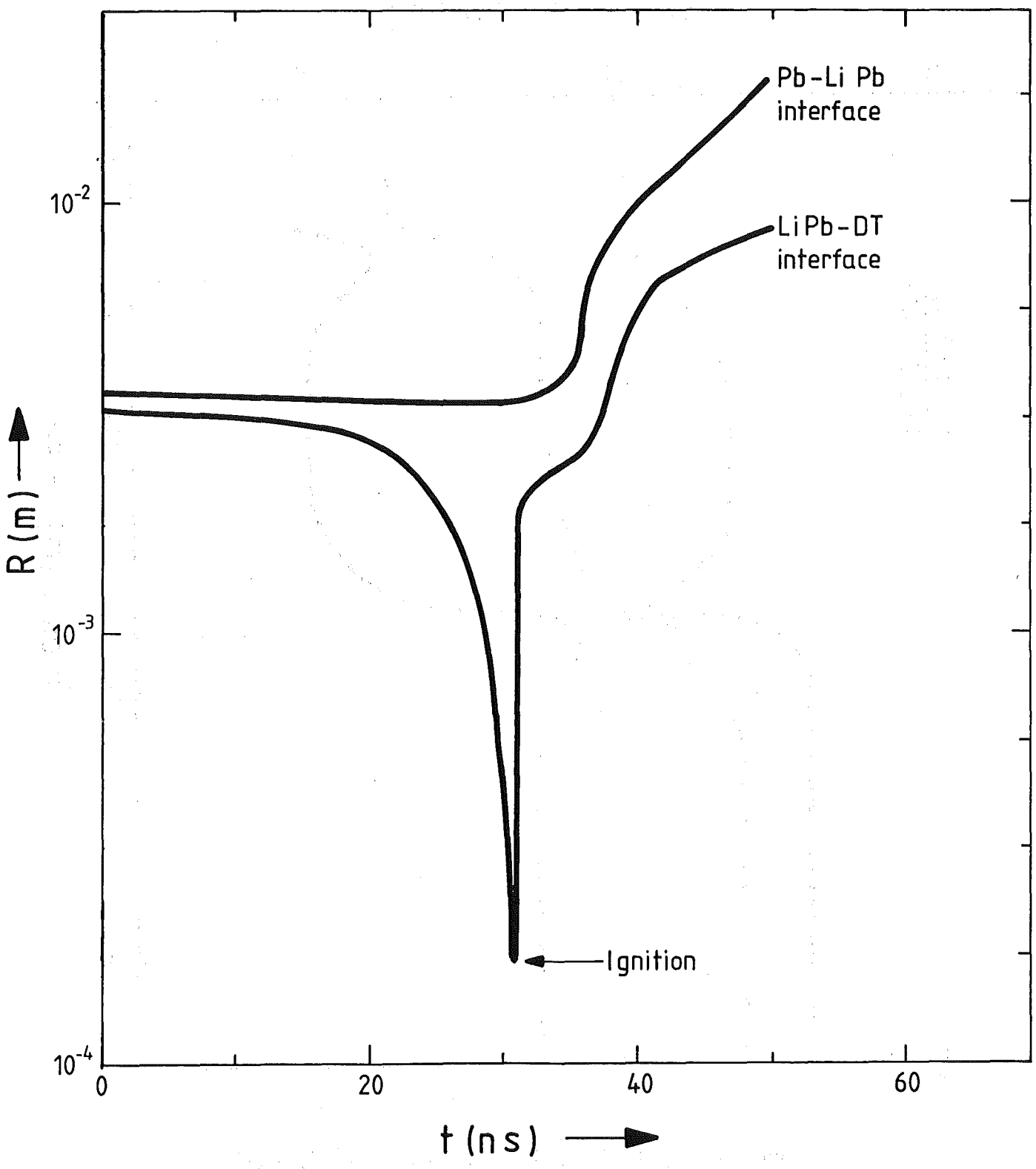

Fig. 11: Trajectories of material interfaces during compression and burn

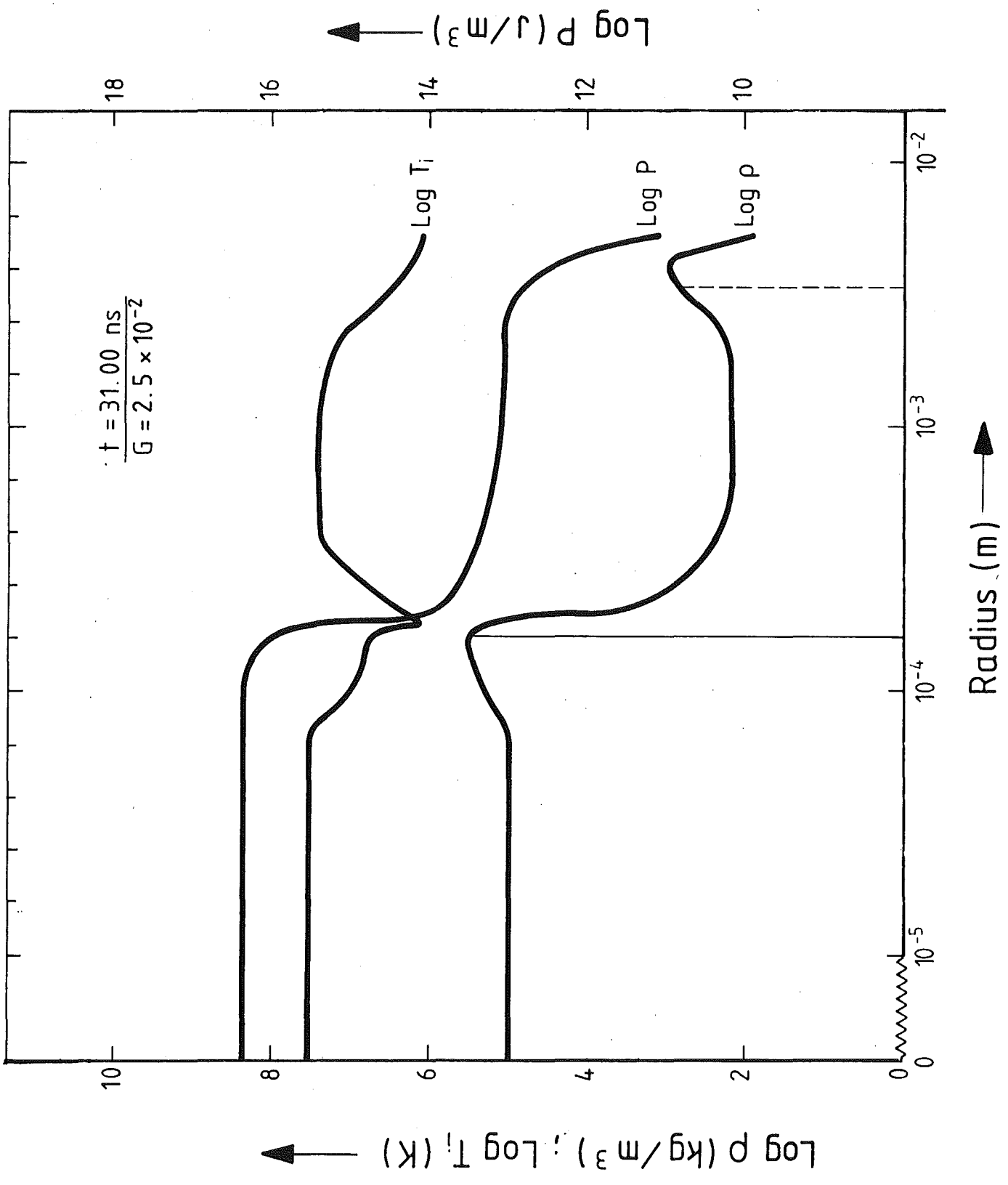

Fig. 12: Density, temperature, and pressure as a function of target radius at ignition

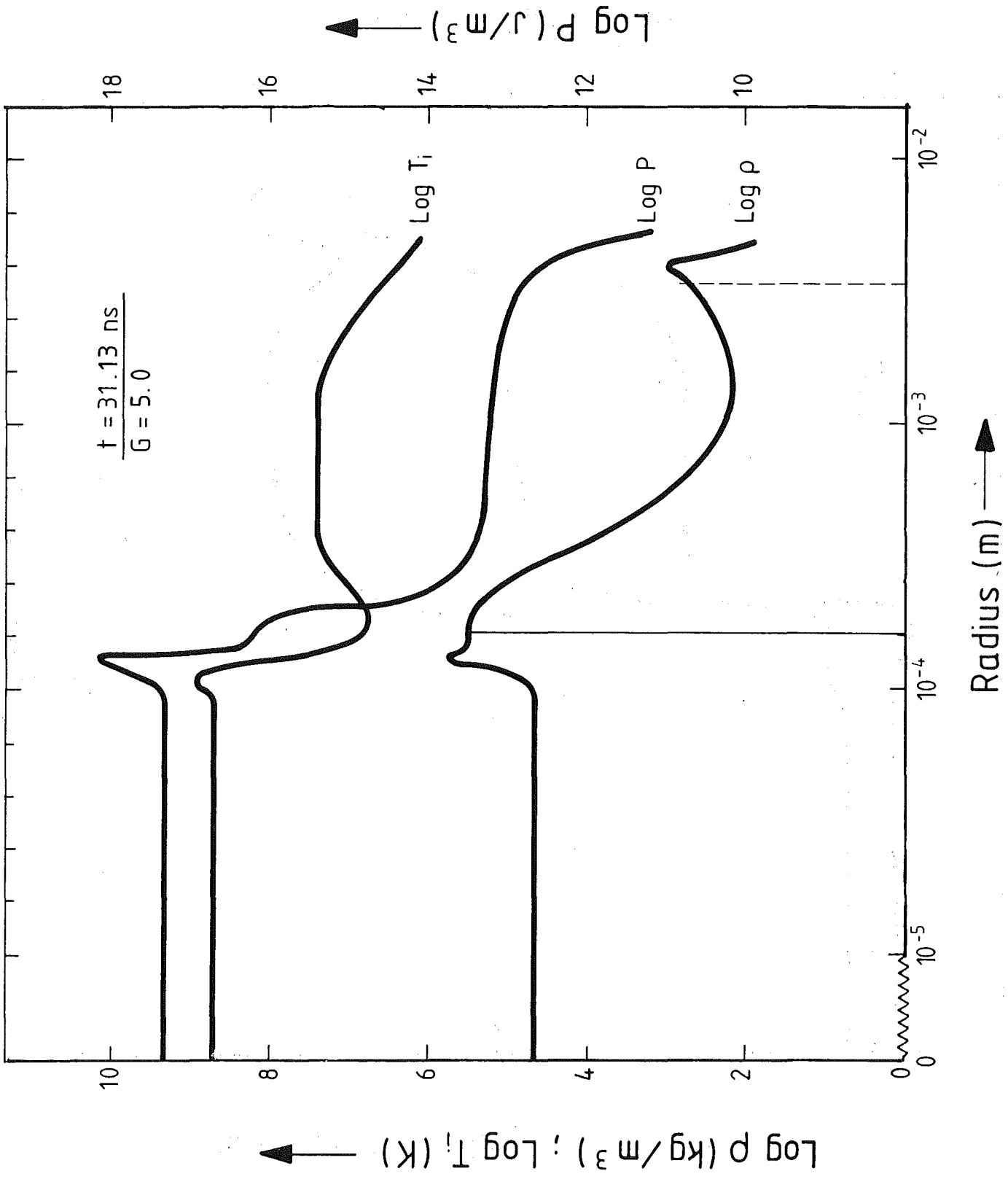

Fig. 13: As Fig. 12, 130 ps after ignition

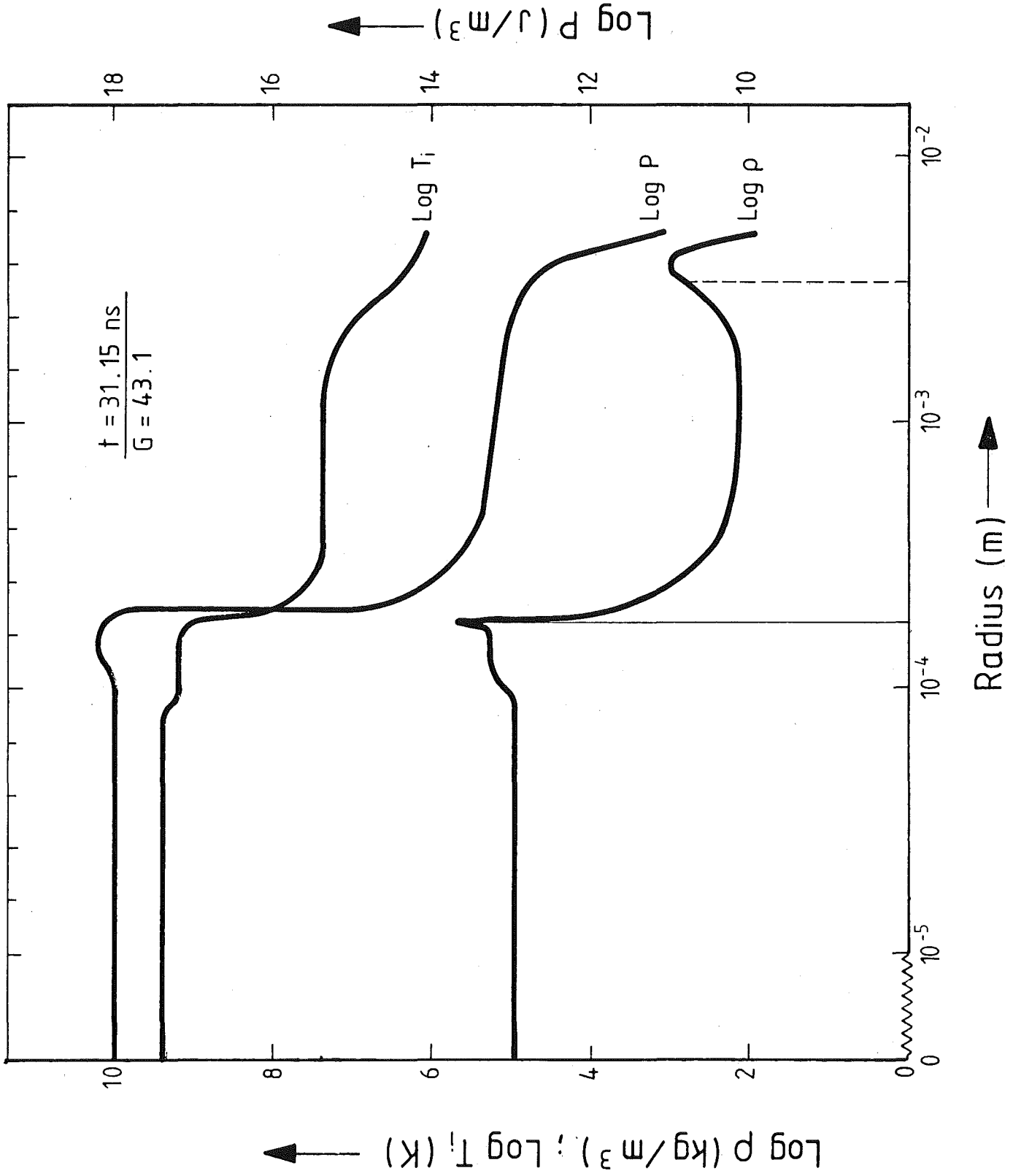

Fig. 14: As Fig. 12, 150 ps after ignition

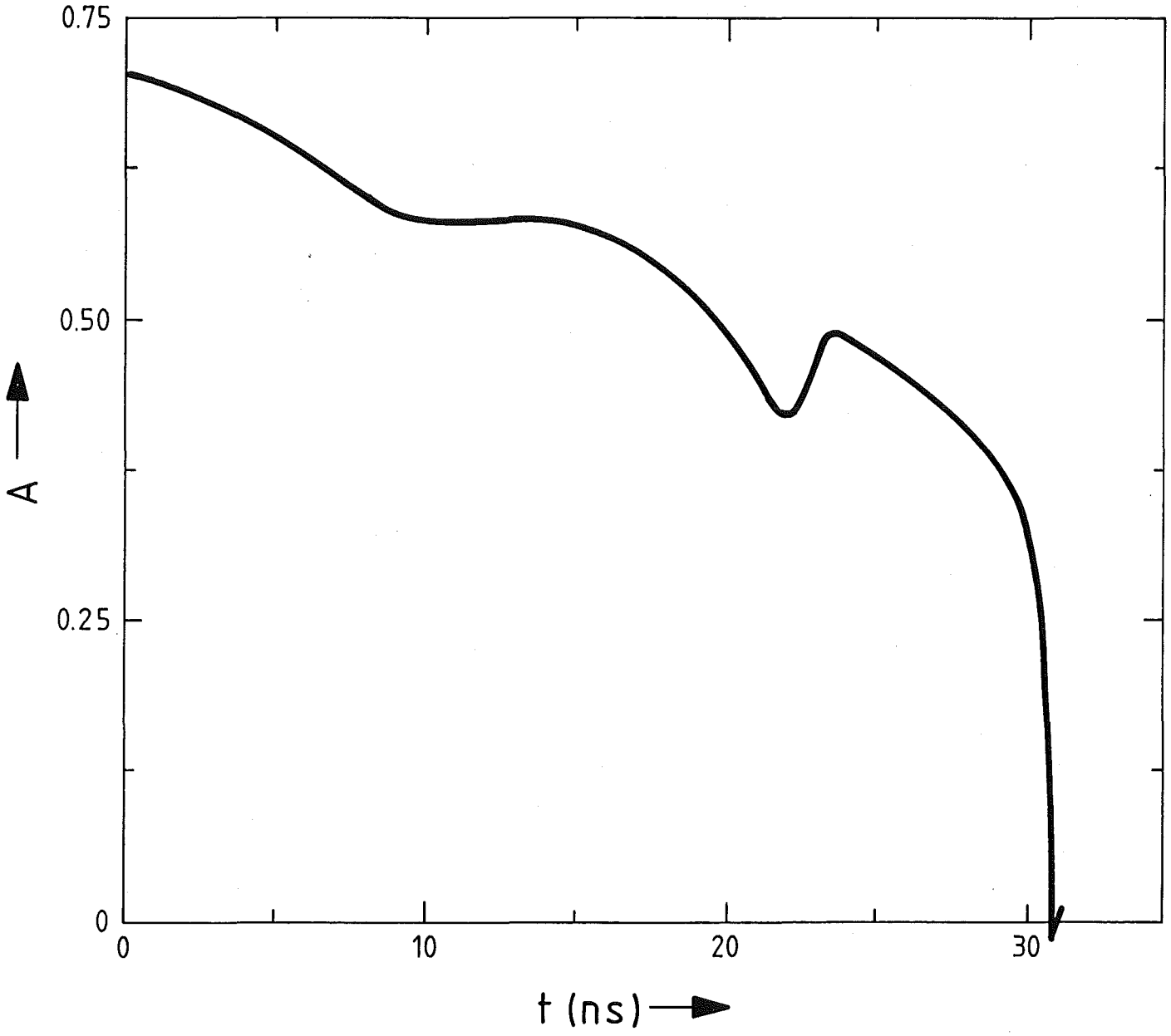

Fig. 15: Atwood number at pusher-fuel interface as a function of time

6. Discussion and conclusion

An advanced and extended version of the well-known MEDUSA code has been transformed into a pellet design code suitable for heavy ion beam fusion pellets. It has been stressed that the results produced by oversimplified codes with insufficient physics cannot be trusted. In particular an ad hoc equation of state would lead to thermodynamic inconsistency, and would also yield wrong specific heats and compressibilities. The EOS is vital because it determines to what extent matter can be compressed, and how much energy is needed to do this. Also because the sound velocity is determined from the EOS, the EOS determines the time scale of the whole implosion. The detailed behaviour of strong shocks is also determined by the EOS. Hence with a false EOS, pellets of the wrong size and structure are likely to be designed. Radiation transport is also important in the design of pellets as this can cause preheat of the DT, losses from the surface of the pellet and is important for the propagation of the burn. The HIBALL pellet has been designed to minimize the deleterious effects of radiation transport.[7,38]

The energy deposition of ions in ICF pellet materials has been calculated. A code has been developed which is suitable for the deposition of light and heavy ion beams. Detailed calculations show that range shortening by up to a factor 2 occurs for both heavy and light ions. For heavy ions the deposition profile becomes more peaked as the temperature of the material rises. Typical deposition profiles for the HIBALL pellet materials and the HIBALL pellet itself are presented.

The credibility of the MEDUSA code as a pellet design code has been established by reproducing results obtained by Bangerter for a 1 mgm pellet design. This pellet has then been successfully scaled up using an $m^{1/3}$ law, to 4 mgms of DT. Detailed implosion, ignition and burn phase calculations are presented for this 4 mgm HIBALL reactor study pellet. The gain of this pellet is 97, with an input energy of 7.4 MJ and an output energy of 715 MJ.

Detailed tuning and use of a more carefully tailored pulse is expected to increase the gain and decrease the input energy, while still producing over 500 MJ of energy. We found that the gain of the 4 mgm pellet is less sensitive to changes in the ion beam range and the pulse parameters than the 1 mgm pellet. Larger pellets are hence less sensitive to parameter changes such as ion beam range, so that range shortening will not have such an effect. Range shortening could be compensated for by ramping the voltage of the incoming ions.

The HIBALL pellet design has therefore many attractive features. It is a high gain pellet, and needs reasonable values of input energy and power. It is a relatively simple pellet, which would make construction reasonably easy, and would also keep the cost down because it contains no expensive materials. The pellet materials are compatible with the rest of the reactor design, in particular the coolant materials. Since the density of the high Z tamper is low, it produces minimal radioactivity. The target is over 7 mms in diameter and so focussing problems will not be too hard to overcome. Finally the target is reasonably stable to pusher-fuel instabilities.

Acknowledgements

The authors would like to thank Dr. G. Keßler for suggesting this work in connection with the HIBALL reactor study.
We would also like to thank Dr. R. Fröhlich for many useful discussions. We would like to acknowledge the help of Dr. Zinamon of the Weizmann Institute, Israel, with the energy deposition work. We also wish to thank Mr. N. Moritz for help with the computing work for the energy deposition code.

7. References

1. HIBALL. "A Joint Federal Republic of Germany - University of Wisconsin conceptual heavy ion beam fusion reactor design study", Kernforschungszentrum Report, KfK-3202 and University of Wisconsin Report, UWFDM-450, (1981)

2. J. P. Christiansen, D. E. T. F. Ashby, and K. V. Roberts, "MEDUSA, a one-dimensional laser fusion code", Computer Physics Communications 7, 271, (1974).

3. R. G. Evans, Rutherford Internal Laboratory report, unpublished, private communication.

4. A. R. Bell, "New equation of state for MEDUSA", Rutherford Laboratory report, RL-80-091, (1980).

5. N. A. Tahir, "Simulation studies of laser compression of matter", PhD Thesis, Glasgow University, 1978.

6. N. A. Tahir and E. W. Laing, "Ionization effects in laser produced plasmas", Phys. Lett. 79A, 321, (1980).

7. R. Bangerter and D. Meeker, "Ion beam inertial fusion target designs", LLL Report, UCRL-78474, (1976).

8. D. Henderson, private communication.

9. For information about EOS tables see "J. Kerley et al., "An invitation to participate in the LASL EOS Library", published by Los Alamos Scientific Laboratory, (1980)

10. N. A. Tahir, E. W. Laing, and D. J. Nicholas, "A radiative diffusion model for laser-compression simulations", Rutherford Laboratory report, RL-80-048, (1980).

11. N. A. Tahir and E. W. Laing, "Radiation effects in laser compression simulations", Plasma Physics, 22, 1113, (1980).

12. N. A. Tahir and E. W. Laing, "Radiation effects in gas filled microballoons", Phys. Letts. 77A, 430, (1980).

13. N. A. Tahir, E. W. Laing and D. J. Nicholas, "A multi-group treatment of radiation transport", Rutherford Laboratory report, RL-80-083, (1980).

14. D. Kershaw, "The incomplete Cholesky-conjugate gradient method for the iterative solution of systems of linear equations", J. Comp. Phys., 26, 43, (1978).

15. G. A. Moses, "Laser fusion hydrodynamic calculations", Nucl. Sci. and Eng., 64, 49, (1977).

16. J. S. Clarke, H. N. Fischer, and R. J. Mason, "Laser-driven implosion of spherical DT targets to thermonuclear burn conditions", Phys. Rev. Lett., 30, 89, (1972).

17. E. Nardi, E. Peleg, and Z. Zinamon, "Energy deposition by fast protons in pellet fusion targets", Phys. Fluids 21, 574, (1978).

18. E. Nardi and Z. Zinamon, "Energy deposition by relativistic electrons in high temperature targets", Phys. Rev. A18, 1246, (1978).

19. L. D. Landau and E. M. Lifschitz, Quantum Mechanics, Pergamon Press, Oxford (1965).

20. H. A. Bethe, "Quantenmechanik der Ein und Zwei Elektronen-probleme", in Handbuch der Physik, Springer, Vol. 24, 273, (1933).

21. R. Latter, "Temperature behaviour of the Thomas-Fermi statistical model for atoms", Phys. Rev. 99, 1854, (1955).

22. H. A. Bethe, "Zur Theorie des Durchgangs schneller Korpuskularstrahlen durch Materie", Ann. Phys. 5, 325, (1930).

23. N. Bohr, "On the decrease of velocity of swiftly moving electrified particles in passing through matter", Phil. Mag. 30, 581, (1915).

24. D. Pines and P. Nozières, "The theory of quantum liquids", Benjamin, N.Y., (1966).

25. D. Pines, "Elementary excitations", Benjamin, N.Y., (1965).

26. S. Doniach and E. Sondheimer, "Green's functions for solid state physicists", Benjamin, (1972).

27. M. D. Brown and C. D. Moak, "Stopping powers of some solids for 30 - 90 MeV ^{238}U ions", Phys. Rev. B6, 90, (1972).

28. S. Chandrasekhar, Principles of Stellar Dynamics, Dover, p. 251, (1960).

29. K. A. Long, "Energy deposition of ions and α-particles in ICF targets", in: Untersuchungen zur Eignung von Schwerionenstrahlen für den Trägheitseinschluß, Jahresbericht 1980, p. 29, GSI 81-3, (1981).

30. T. A. Mehlhorn, "A finite temperature model for ion energy deposition in ion-driven ICF targets", SAND80-0038, (1981).

31. J. Nuckolls, L. Wood, A. Thiessen, and G. Zimmerman, "Laser compression of matter to super-high densities: Thermonuclear (CTR) applications", Nature, 239, 139, (1972).

32. R. E. Kidder, "Laser driven compression of hollow shells: Power requirements and stability limitations", Nucl. Fusion, 16, 3, (1976).

33. D. E. T. F. Ashby, "Laser-induced compression of thin shells and uniform spheres: A theoretical comparison", Nucl. Fusion, 16, 231, (1976).

34. S. E. Bodner, "Critical elements of high gain laser fusion", NRL Report 4453, (1981).

35. R. E. Kidder, "Energy gain of laser-compressed pellets: A simple model calculation", Nucl. Fusion 16, 405, 1976.

36. R. E. Kidder, "Theory of homogeneous isentropic compression and its application to laser fusion", Nucl. Fusion, 14, 53, (1974).

37. R. E. Kidder, "Laser-driven isentropic hollow-shell implosions: The problem of ignition", Nucl. Fusion, 19, 223, (1979).

38. R. Bangerter, "Fusion Target Design", LLL Report, UCRL-82026, (1978).

39. G. S. Fraley, E. J. Linnebur, R. J. Mason, and R. L. Morse, "Thermonuclear burn characteristics of compressed DT microspheres", Phys. Fluids, 17, 474, (1974).

40. R. C. Kirkpatrick, "An overview of design space for small fusion targets", Nucl. Fusion, 19, 69, (1979).

41. R. C. Kirkpatrick and J. C. Wheeler, "The Physics of DT ignition in small fusion targets", Nucl. Fusion, 21, 389, (1981).